Spectroscopic and molecular modeling probing of biophysical influence of β-casein nano-protein on adrenaline and arachidonoyl adrenaline

Hanieh Abolhassani, Abdol-Khalegh Bordbar, Najmeh Fani, Zahra Adibipour, Mehdi Sahihi, Elham Sattarinezhad, Samira Gholami, Maryam Atrian

Spectroscopic and molecular modeling probing of biophysical influence of β-casein nano-protein on adrenaline and arachidonoyl adrenaline

- Hanieh Abolhassani,
- Abdol-Khalegh Bordbar,
- Najmeh Fani,
- Zahra Adibipour,
- Mehdi Sahihi,
- Elham Sattarinezhad,
- Samira Gholami &
- Maryam Atrian

Abdol-Khalegh Bordbar bordbar@chem.ui.ac.ir; akbordbar@gmail.com
Department of Chemistry, University of Isfahan, Isfahan 81746-73441, Iran

Abstract

The interaction mechanism of adrenaline and arachidonoyl adrenalin with β-casein milk protein as a nano-carrier was investigated by fluorescence spectroscopy, molecular docking, and molecular dynamics simulation approaches. The results of fluorescence studies and thermodynamic parameters revealed the negative values of enthalpy and entropy changes for both compounds which illustrate the vital role of hydrogen bond and van der Waals interaction in stabilizing protein–ligand complexes. The docking studies showed that adrenaline binds to several polar and non-polar residues in the inner hydrophobic core of β-casein with binding energy of $-27.25\ \text{kJ mol}^{-1}$ but arachidonoyl adrenalin binds in a core near the surface of this protein with the binding energy of $-28.67\ \text{kJ mol}^{-1}$. Finally, the molecular dynamics simulation results suggested that the interactions between protein and both compounds are very stable and during the whole simulation time no significant protein structure changes were observed, consequently β-casein can be considered as a suitable carrier for adrenaline and arachidonoyl adrenalin.

Introduction

When a person perceives a situation as threatening or exciting, the hypothalamus in the brain signals to the adrenal glands to produce adrenalin (AD) by transforming the amino acid tyrosine into dopamine. In fact, the oxygenation of dopamine produces noradrenaline (norAD), which is then converted into AD. AD as a catecholamine is structurally similar to norAD and is the *N*-methylated product of this compound. Both the adrenal hormones have the same chemical precursors and they both are vasoconstrictors [1] but AD is 20–100 times more active than norAD. It has been shown that various forms of stress, thermal burn, muscular exercise, centrifugation, and trauma activate the sympatho-adrenal system and this activation is manifested by an increase in the urinary output of AD and norAD [2]. These effects can reverse severe low blood pressure, wheezing, severe skin itching, hives, and other symptoms of an allergic reaction. It was shown that AD does this by its effects on alpha and beta receptors [3]. AD binds to these receptors on the heart and arteries and increases heart rate and respiration. Moreover, this hormone inhibits the production of insulin and stimulates the synthesis of sugar and fat by binding to the receptors on the pancreas, liver, muscles and fatty tissue. Arachidonoyl adrenalin (AA-AD) is strictly related to endocannabinoid/endovanilloid *N*-arachidonoyl dopamine (NADA) as an endogenous

capsaicin-like compound. NADA displays high potency for transient receptor potential vanilloid type 1 (TRPV1) channels and cannabinoid type 1 receptors (CB1) [4, 5]. Endocannabinoids modulate a multitude of physiological functions which is only partially based on their binding to the classical cannabinoid receptors CB1 and CB2. These signaling lipids have been implicated in the regulation of the immune system [6], the gastrointestinal tract [7] and the cardiovascular system [8]. Moreover, endocannabinoids have psychoactive effects on the central nervous system (CNS) of human body [9].

Experimental studies showed that extreme amounts of circulating catecholamines are oxidized to aminochromes that could affect their physiological benefits and cause some disorders in body. Moreover, formation of oxyradicals during the oxidation process may result in sudden cardiac death [10]. The binding of catecholamines to nano-carrier proteins can protect them from oxidation, increase drug efficacy, solubility, and stability and can decrease drug toxicity [11]. Hence, it would be of interest to obtain insight into the binding mechanism of these compounds with some nano-carrier proteins.

Caseins are a family of phosphoproteins which commonly make up 80% of the proteins in cow's milk and between 20 and 45% of the proteins in human milk [12]. Bovine beta-casein (βCN) that constitutes up to 45% of the casein of bovine milk is a single-chain protein containing 209 residues with molecular weight of 23.983 kDa. βCN is a highly amphiphilic calcium-sensitive phosphoprotein which consists of a hydrophilic N-terminal part with a cluster of five phosphoryl residues and a hydrophobic C-terminal part [13]. This protein has been known as a dynamic protein with non-compact and flexible conformation [14]. Many studies have demonstrated that βCN micelles may be utilized as natural nano-delivery vehicles for lipid-soluble drugs. Moreover, βCN evolved to be easily digestible and this basic nano-carrier is expected to readily release its chemotherapeutic compound in the stomach [15]. Some studies have investigated the binding properties of some drug candidates with bovine βCN nanoparticles using various experimental and computational techniques [16].

In this paper, fluorescence spectroscopy, molecular docking and molecular dynamics (MD) simulation methods have been used for investigation of the interaction mechanism between AD and AA-AD (Fig. 1) with bovine βCN nano-carrier. Structural information regarding binding modes, binding energies, and the effect of AD and AA-AD on the protein stability and protein structure are stated here.

Fig. 1 Chemical structures of AD and AA-AD

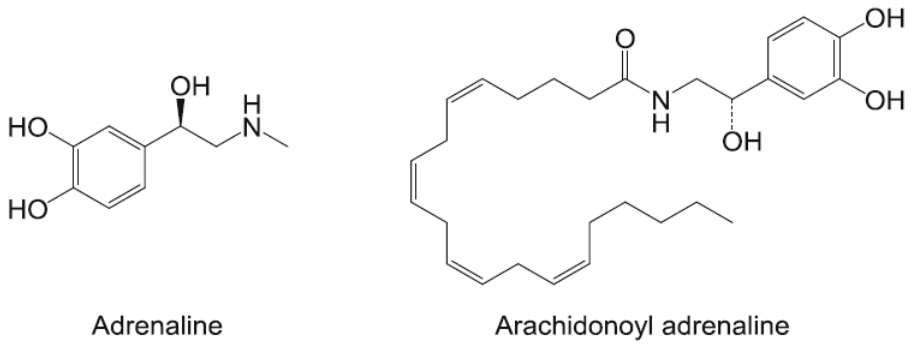

Results and discussion

Fluorescence spectroscopy

Measuring the intrinsic fluorescence of protein in the presence of different concentrations of ligands is a way in which we can compute binding parameters. βCN has one Trp residue that the

intrinsic fluorescence of its indole chromospheres is chiefly sensitive to their polarity of environments. Essentially, this Trp residue is placed in a primarily hydrophobic domain of βCN, and can provide important information about the interaction and formation of AD–βCN and AA-AD–βCN complexes. As shown in Figs. 2a and 3a, when a fixed concentration of βCN was titrated with various amounts of AA and AA-AD, a remarkable increase of the fluorescence intensity was observed. The enhancement of fluorescence is based on the photophysical phenomenon whereby the intensity of a fluorophore increases upon proximal binding of a ligand. There are two different mechanisms, static and dynamic, for enhancing of fluorescence intensity. In the static mechanism, the ligand binds to protein and a complex with higher molar absorptivity formed while in the dynamic mechanism, the ligand interacts with excited state of protein and reduced the rate constant of irradiative mechanisms. By calculating the surfaces under the fluorescence plots and using Eq. (1) the increasing constants can be estimated [17, 18].

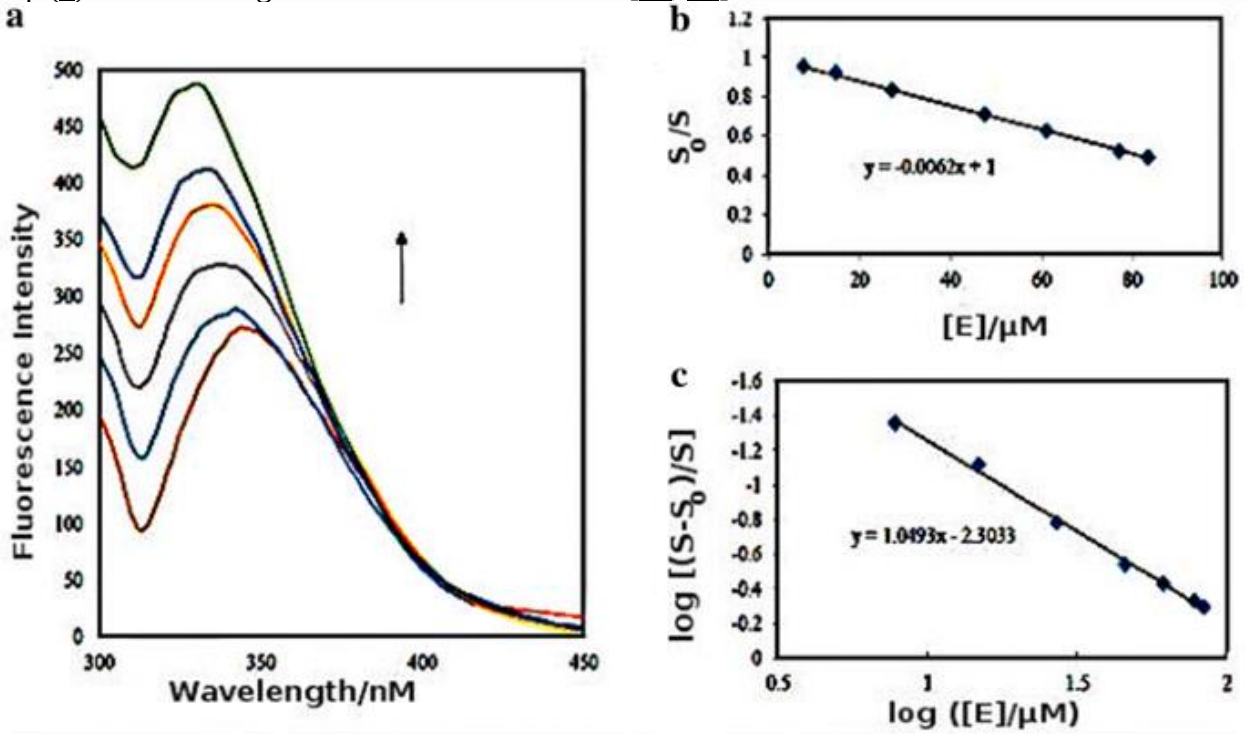

a Fluorescence increase of βCN solution by AD in PBS, pH 7, T = 293 K, λ_{ex} = 295 nm, and [βCN] = 16.30 μM. The concentration of AD is increased in the direction of arrow. **b** The variation of S_0/S versus total concentration of AD. **c** The variation of log $[(S_0 - S)/S]$ *vs*. log [E]

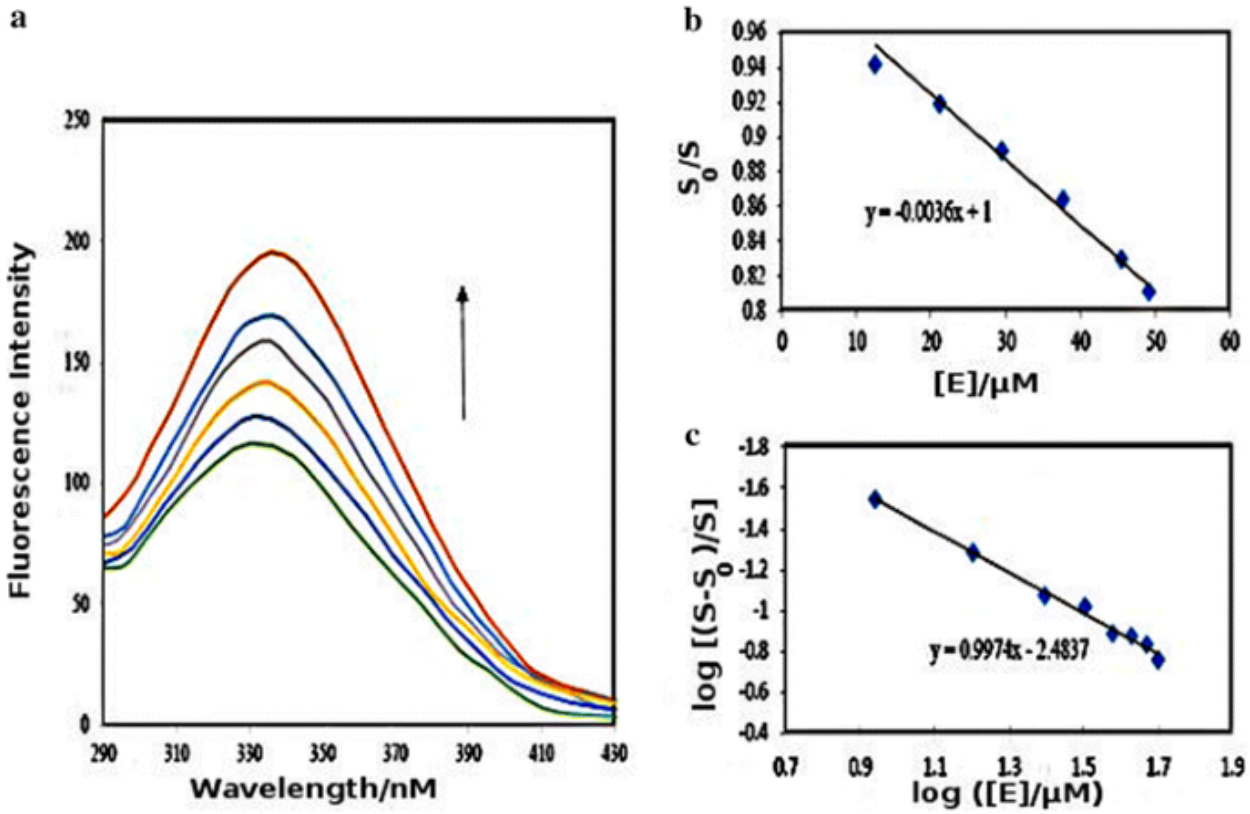

a Fluorescence increase of βCN solution by AA-AD in PBS, pH 7, T = 293 K, λ_{ex} = 280 nm, and [βCN] = 16.30 μM. The concentration of AA-AD is increased in the direction of arrow. **b** The variation of S_0/S vs. total concentration of AA-AD. **c** The variation of log $[(S_0 - S)/S]$ *vs*. log $[E]$

$$S_0/S = 1 - K_E\,[E] \qquad (1)$$

where S_0 and S are the total area under the emission spectrum in the absence and presence of ligand, $[E]$ is the ligand concentration, and K_E is the increasing constant. Plots of S_0/S versus [AD] and [AA-AD] at 293 K are shown in Figs. 2b and 3b, respectively. The calculated K_E at four temperatures from 293 to 308 K for AD and AA-AD are presented in Table 1. The K_E values decrease with the increase of temperature which demonstrates static mechanism for interaction between these ligands with βCN.

Table 1 Increasing constants for interaction of AD and AA-AD with βCN in PBS, pH 7

	T/K	$K_E \times 10^{-3}/M^{-1}$	R^2
βCN-AD	293	6.210 ± 0.074	0.9988
	298	6.080 ± 0.073	0.9980
	303	5.820 ± 0.077	0.9975
	308	5.100 ± 0.094	0.9953
βCN-AA-AD	293	3.560 ± 0.113	0.9984
	298	3.490 ± 0.026	0.9993
	303	2.890 ± 0.178	0.9845
	308	1.720 ± 0.028	0.9932

If there are n substantive binding sites on the surface of protein to accommodate the ligand molecules, the equilibrium between free and bound molecule is given by the following equation [17] where K_a is the associative binding constant:

$$\ln[(S_0 - S)/S] = \ln K_a + n \ln[E] \quad (2)$$

The corresponding plots of this equation are shown in Figs. 2c and 3c for AD and AA-AD, respectively. Binding constants and number of binding sites for interaction of AD and AA-AD with βCN are listed in Table 2.

Table 2 Binding constants and number of binding sites for interaction of AD and AA-AD with βCN in PBS, pH 7

	T/K	$K_b \times 10^{-3}$/M^{-1}	R^2	n
βCN-AD	293	4.981 ± 0.458	0.9971	1.049 ± 0.025
	298	3.890 ± 0.376	0.9972	1.120 ± 0.027
	303	2.489 ± 0.122	0.9994	1.183 ± 0.013
	308	1.221 ± 0.091	0.9969	1.314 ± 0.051
βCN-AA-AD	293	3.281 ± 0.256	0.9930	0.997 ± 0.034
	298	1.480 ± 0.143	0.9954	1.244 ± 0.042
	303	0.990 ± 0.148	0.9972	1.314 ± 0.065
	308	0.742 ± 0.126	0.9965	1.253 ± 0.074

The calculated binding constant for interaction of AD and AA-AD with βCN is lower than the binding constants of curcumin, diacetyl curcumin, and quercetin with this protein [16, 19, 20]. Thermodynamic parameters such as the standard Gibbs free energy, ΔG^0, the standard molar enthalpy, ΔH^0, and the standard molar entropy, ΔS^0, can be estimated by analyzing K_a values at different temperatures using the following equations:

$$\Delta G^0 = -RT \ln K_a \quad (3)$$

$$\Delta H^0 = \mathrm{d}(\Delta G^0/T)/\mathrm{d}(1/T) \quad (4)$$

$$\Delta S^0 = (\Delta H^0 - \Delta G^0)/T \quad (5)$$

where R and T are gas constant and the absolute temperature, respectively. If the temperature does not vary considerably, the standard enthalpy change (ΔH^0) can be regarded as a constant. Plots of $\Delta G^0/T$ *vs.* $1/T$ for AD and AA-AD are shown in Fig. 4 and calculated thermodynamic parameters are reported in Table 3.

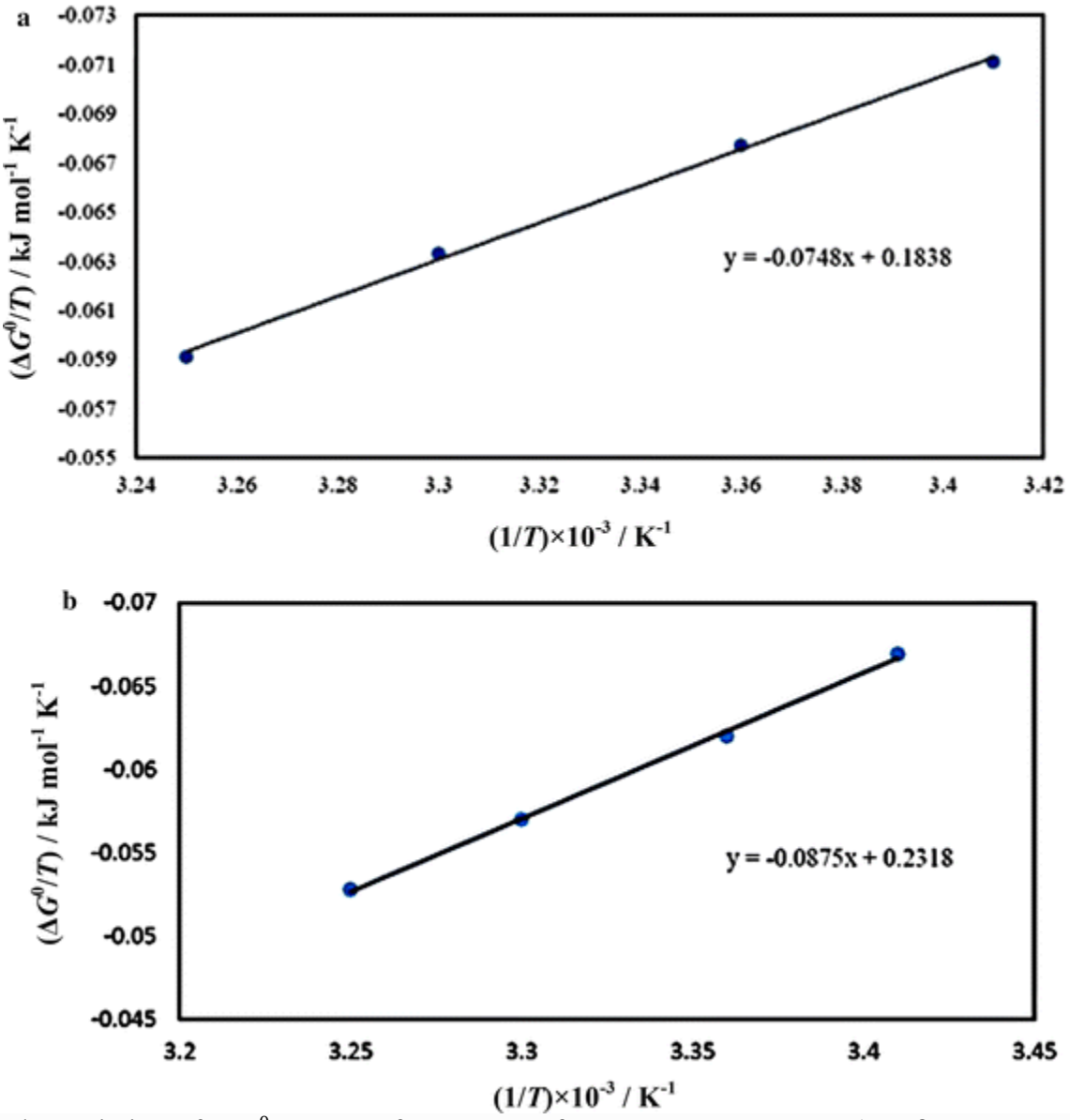

The variation of $\Delta G^0/T$ *vs.* $1/T$ for binding of AD (**a**) and AA-AD (**b**) to βCN at pH 7 in PBS buffer

Table 3 Thermodynamic parameters for the association of AD and AA-AD with βCN

	T/K	Δ*G*°/kJ mol^{-1}	Δ*H*°/kJ mol^{-1}	Δ*S*°/J mol^{-1}
βCN-AA	293	− 20.738 ± 0.224	− 74.790 ± 2.373	− 183.795 ± 8.134
	298	− 20.480 ± 0.240	− 74.790 ± 2.373	− 179.496 ± 8.004
	303	− 19.698 ± 0.126	− 74.790 ± 2.373	− 179.116 ± 7.845
	308	− 18.200 ± 0.192	− 74.790 ± 2.373	− 181.071 ± 7.734
βCN-AA-AD	293	− 19.721 ± 0.280	− 87.530 ± 2.332	− 231.430 ± 8.011
	298	− 18.085 ± 0.377	− 87.530 ± 2.332	− 293.664 ± 7.927
	303	− 17.376 ± 0.579	− 87.530 ± 2.332	− 231.531 ± 7.928
	308	− 16.229 ± 0.629	− 87.530 ± 2.332	− 231.496 ± 7.839

The driving forces for interaction of AD and AA-AD with βCN can be concluded from the sign and magnitude of the thermodynamic parameters which were characterized by Ross and Subramanian. They express that hydrophobic force might increase ΔH^0 and ΔS^0 of a system, hydrogen bond and van der Waals interactions decreased them and electrostatic force usually made $\Delta H^0 \approx 0$ and $\Delta S^0 > 0$ [21, 22]. Just as Table 3 shows, negative values of standard free energy explain the spontaneity of the binding reaction and relative high affinity of these ligands to βCN and the negative values of ΔH^0 and ΔS^0 represent an enthalpy-driven process.
In advance, the negative value obtained for ΔH^0 points to the importance of hydrogen binding in the interaction process and the negative values of ΔS^0 shows the van der Waals interactions in solution. Therefore, it can be concluded that both hydrogen bonding and van der Waals interactions play an essential role in the binding of AD and AA-AD to βCN.

Molecular docking study

Docking studies showed that AD and AA-AD bind to several polar and non-polar residues in the inner hydrophobic core of β-casein and in the core near the surface of this protein. Docking results for binding of AD and AA-AD to βCN are shown in Fig. 5. AD is close to some hydrophobic residues in the core of βCN such as Leu31, Ile45, Phe102, Val92, and Phe67. Moreover, this compound is in contact with some polar residues such as Glu106, Gln71, Lys43, and Lys44. AA-AD interacts with hydrophobic residues: Ile202, Tyr195, Val224, Phe205, Val212, Ile222, Phe102, and Ile223 and polar residues: Lys191 and Asp199. Moreover, hydroxyl groups of AD were found to interact with Ile45, Glu106, and Lys43 through hydrogen bonds and nitrogen atom of this compound formed one hydrogen bond with Phe67. The representative build structure derived from the best pose for interactions between AD and βCN has the minimal binding energy of $-27.25\ \text{kJ mol}^{-1}$ and for AA-AD–βCN complex has the minimal binding energy of $-28.67\ \text{kJ mol}^{-1}$. The interaction of the ligands with these residues could change the microenvironment of Trp158 and consequently enhances its quantum yield. The calculated binding energy for interaction of AD and AA-AD with βCN is higher than the binding energies of curcumin, diacetylcurcumin and quercetin with this protein [16, 19, 20].

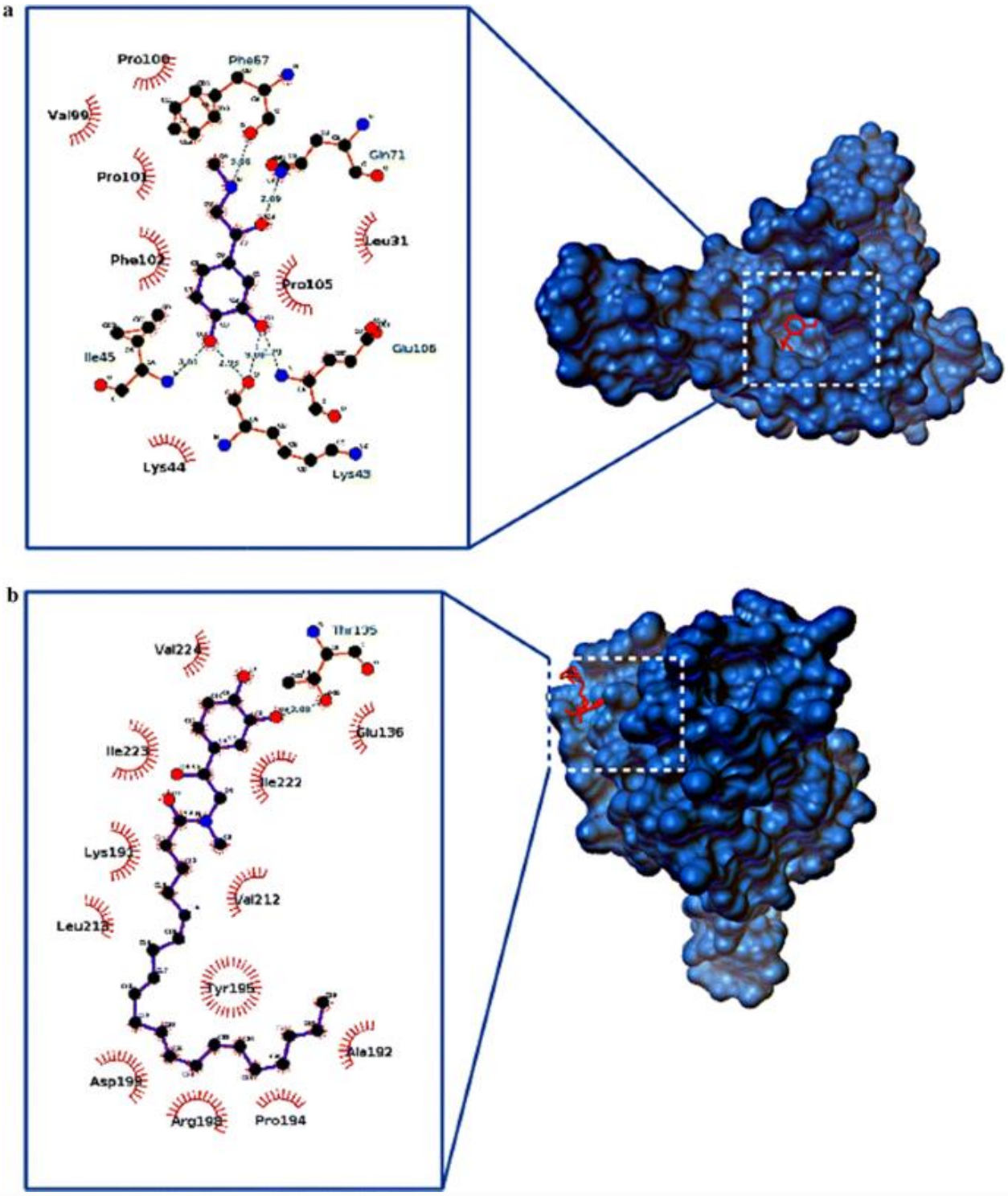

The structure of AD (**a**) and AA-AD (**b**) in the binding site of βCN as a mesh surface image and the schematic description of the environment of ligands bound to protein generated by Ligplot+. Only the more important residues for binding are shown

Molecular dynamics simulation study

The structure with the lowest binding energy from docking calculation was selected to perform another MD simulation (40 ns) on the AD–βCN and AA-AD–βCN complexes. To compare the structural stability of free and bound βCN and ligands and determination of involving interactions, some dynamic structural properties such as root mean square deviations (RMSD), radius of gyration, root mean square fluctuations (RMSF), surface area of protein, and hydrogen bonds have been analyzed. In the following, the details of investigated parameters are explained.

Root mean square deviations (RMSD)

The RMSD of backbone atoms of protein from the initial structure as a function of time have been deliberated to analyze the trajectory stability of free βCN and βCN in complex with AD and AA-AD. As Fig. 6a shows the RMSD of βCN, AD–βCN, and AA-AD–βCN achieve stability after 19, 25, and 17 ns, respectively. Moreover, the mean RMSD values of protein backbone atoms from last 20 ns trajectory were 0.429 ± 0.073, 0.431 ± 0.078, and 0.407 ± 0.070 nm for βCN, βCN–AD, and βCN–AA-AD complexes, respectively.

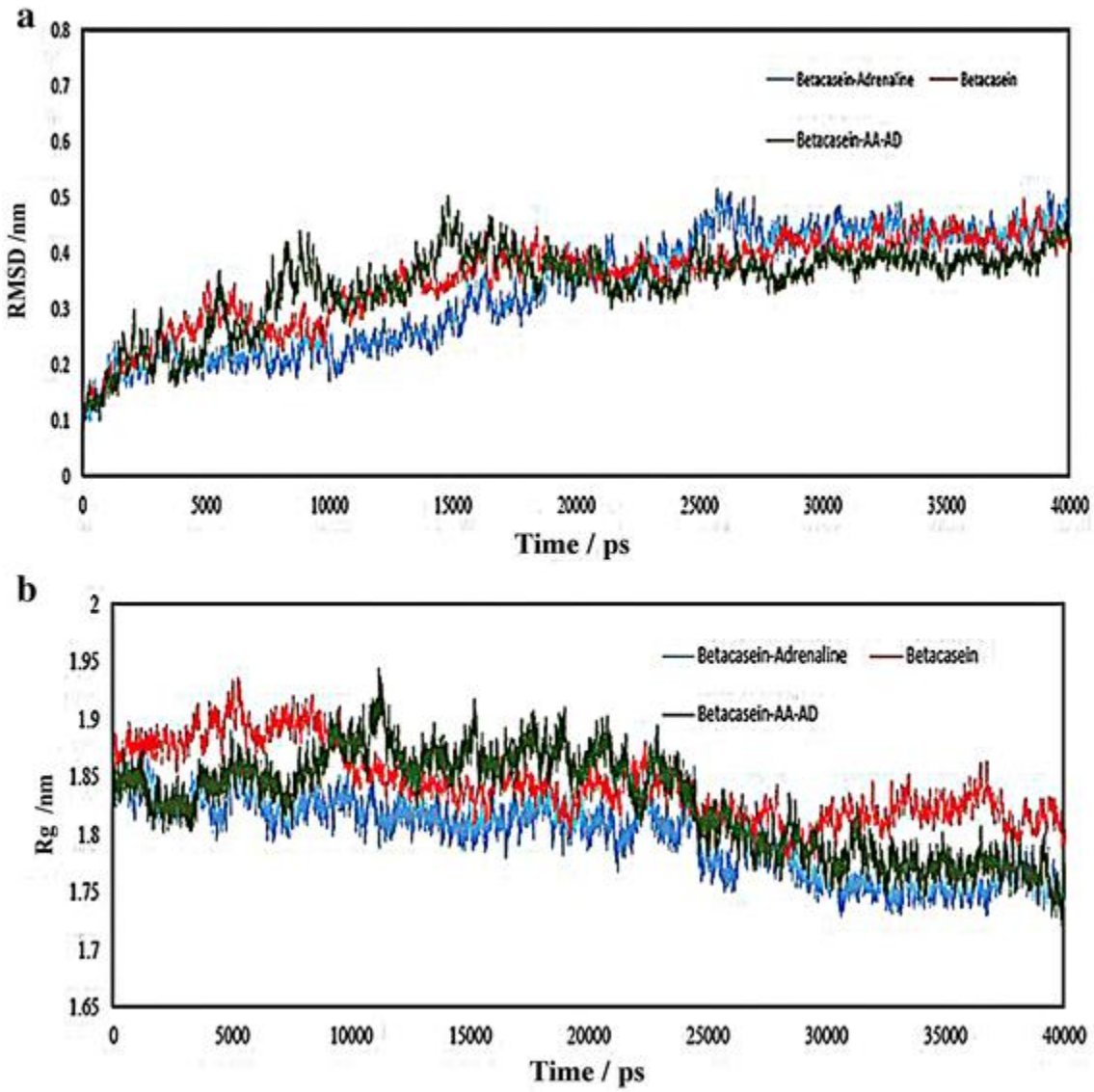

a RMSD (nm) of backbone atoms of βCN in the absence and presence of AD and AA-AD. **b** Time dependence of the radius of gyration (R_g) for the backbone atoms of βCN during the simulation in the absence and presence of AD and AA-AD

Radius of gyration (R_g)

The compactness of protein structure during the MD simulation time was assessed by the radius of gyration (R_g) using g_gyrate command. The R_g for the free and bound form of protein with AD and AA-AD was determined and plotted as a function of time (Fig. 6b). For all cases the R_g values were stabilized at about 20 ns, indicating that the system achieved equilibrium after this time. The values of R_g for bound form of βCN is less than free protein implying the compacting of βCN structure after binding with AD and AA-AD.

Root mean square fluctuations (RMSF)

The time-averaged RMSF values for free and bound βCN were measured to investigate local protein mobility. The results were plotted against residue number at the simulation trajectory and shown in Figs. 7 and 8. RMSF values demonstrate that protein structure in the presence of both ligands remained stable during the simulation.

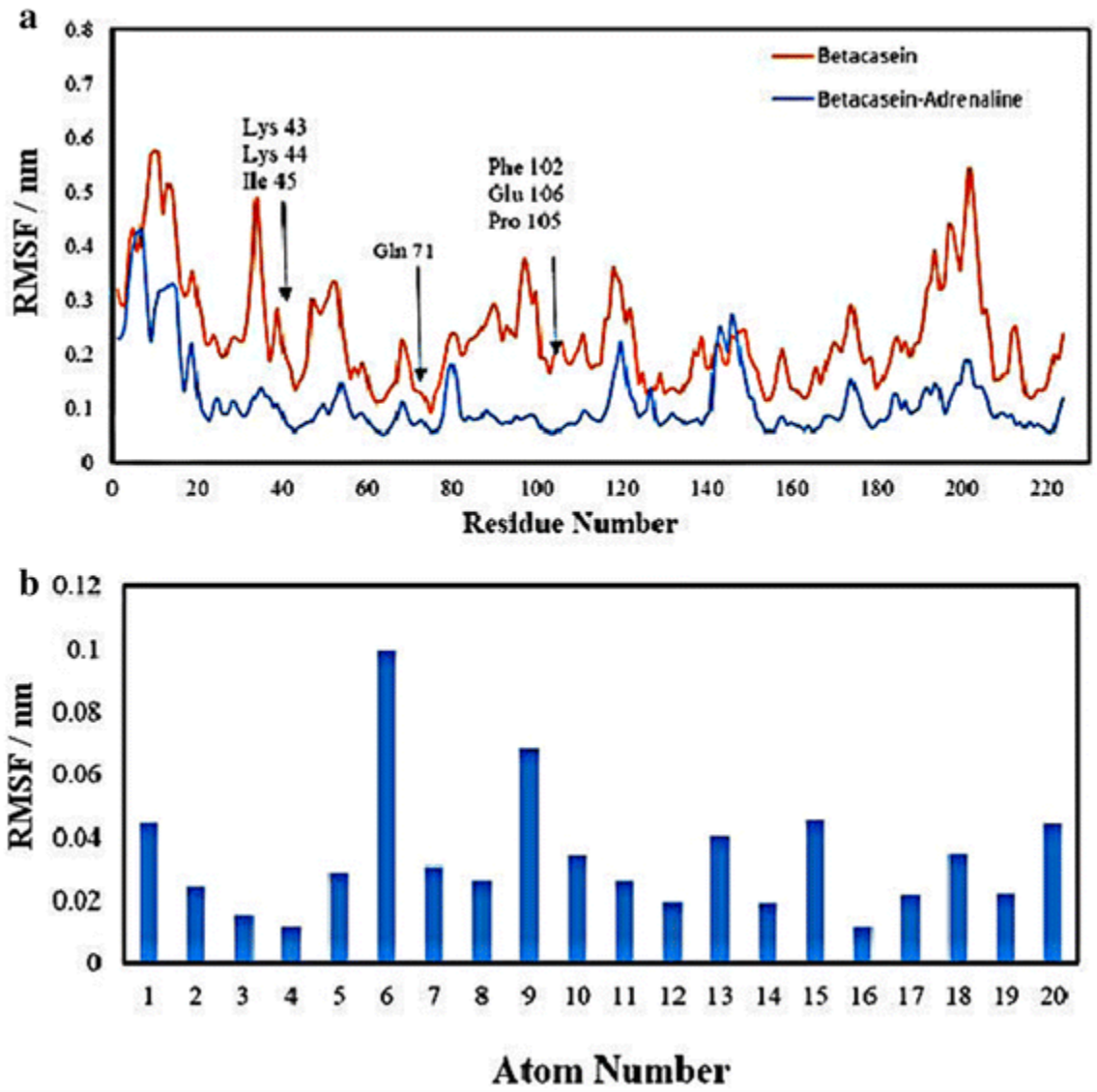

a RMSF of residues of protein from their time-averaged positions for free and bound βCN with AA. **b** RMSF of AD atoms during the simulation time

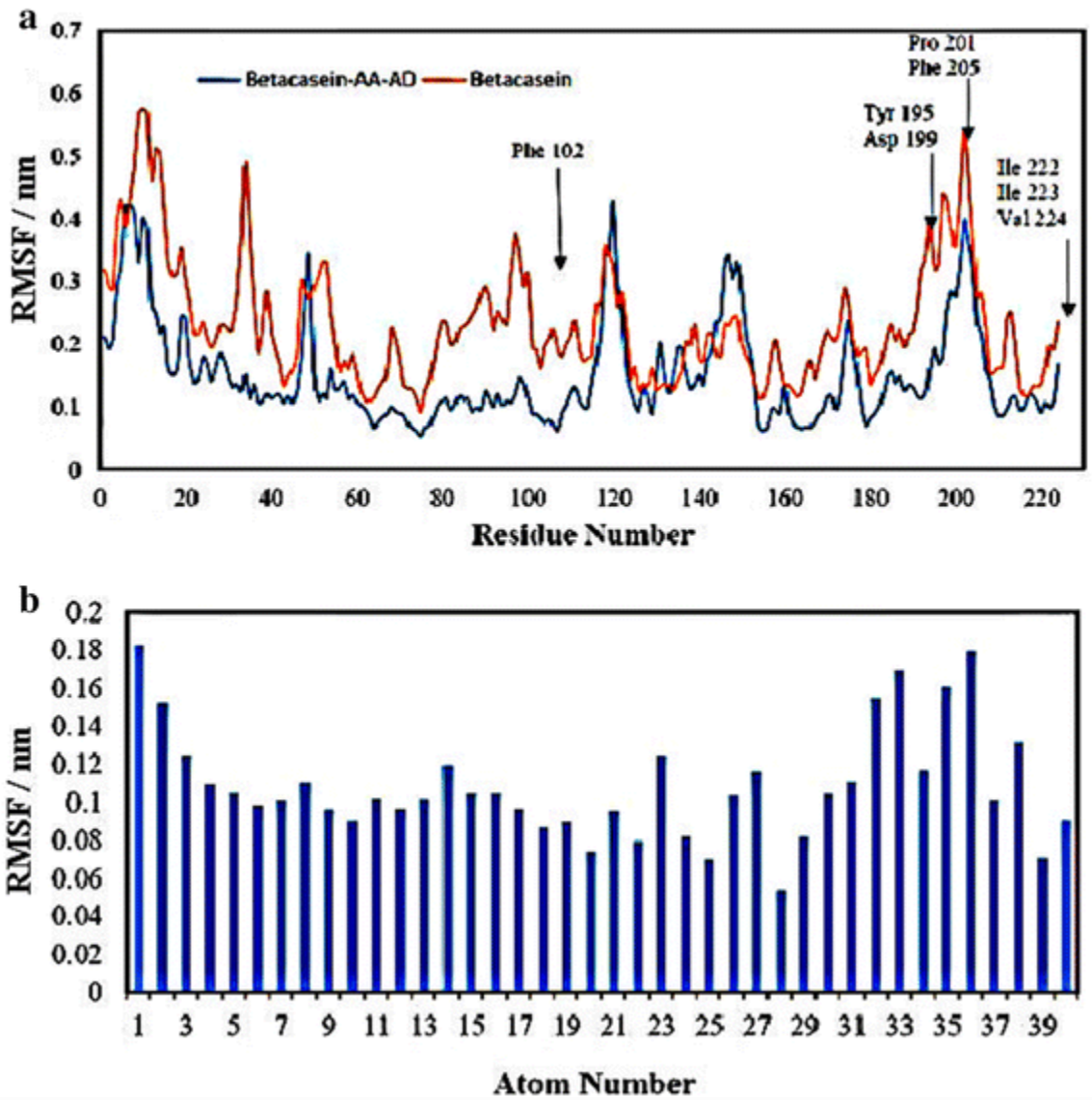

a RMSF of residues of protein from their time-averaged positions for free and bound βCN with AA-AD. **b** RMSF of AA-AD atoms during the simulation time

The particular regions directly in contact with ligands including Leu31, Ile45, Phe102, Val92, Phe67, Glu106, Gln71, Lys43, Pro105, Lys44 residues for βCN–AD, and Ile202, Tyr195, Val224, Phe205, Val212, Ile222, Phe102, Ile223, Pro201, Lys191, Asp199 residues for βCN–AA-AD (pointed in Figs. 7a and 8a, respectively) showed more significant reduction of RMSF that is related to intermolecular interactions of these residues with these ligands. The same residues are in contact with ligands with respect to docking results representing insignificant displacement of ligands inside the binding site during the simulation time.

Surface area of the protein

Another parameter for evaluating a MD simulation is the variation of accessible surface area (ASA) of free and bound forms of protein as function of time to compute hydrophobic, hydrophilic, and total solvent accessible surface area and to judge the stability of the system. Figure 9a shows the area of the protein in the presence and absence of the ligands and indicates that the surface of βCN due to its complexation reduces which is in good agreement with investigation of the radius of gyration.

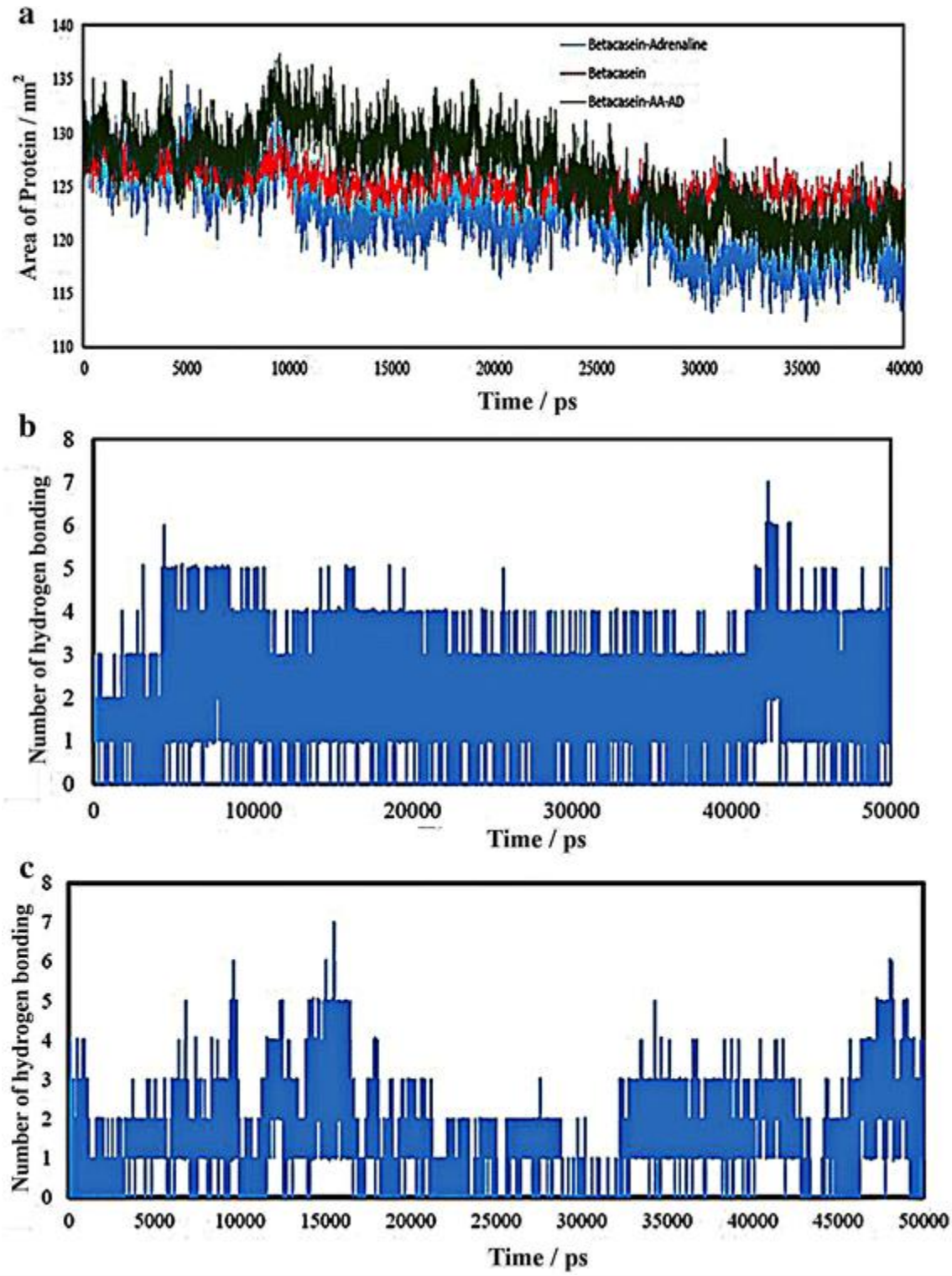

a Total surface area of the protein in the presence and absence of AD and AA-AD. **b** Number of hydrogen bonds that exist in the 40-ns simulation between βCN and AD. **c** Number of hydrogen bonds that exist in the 40-ns simulation between βCN and AA-AD

Accessible surface area values for βCN, βCN–AD, and βCN–AA-AD were obtained as 125.135 ± 1.564, 118.684 ± 3.076, and 122.617 ± 3.567 nm^2, respectively.

Hydrogen bonds

g_hbond is a command to measure the number of hydrogen bonds, hbond distances and angles between molecules or groups through the course of the simulation and these are shown in Fig. 9b, c. As seen in these figures, maximum of seven hydrogen bonds can be exist between ligands and βCN but at most of the time only three and two hydrogen bonds exist in βCN–AD and βCN–AA-AD complexes, respectively, which is in good agreement with the docking results.

Conclusions

In this study, the interactions of AD and AA-AD with βCN were investigated using fluorescence spectroscopy, molecular docking and molecular dynamics simulation studies. The enhancement of fluorescence emission of βCN in the presence of these ligands was observed which represents the changing of microenvironment of Tyr due to the binding of AD and AA-AD. Analysis of fluorescence binding data at various temperatures represents the formation of 1:1 complexes, the higher affinity of AD, enthalpy-driven nature of process and indicates both hydrogen bond and van der Waals interaction as the main driving forces in the binding process. The results of molecular docking calculation represent different binding sites for these ligands located in the hydrophobic domain of the βCN. The obtained RMSD and R_g profiles from MD simulations proved the stability of βCN–ligand complexes and validity of docking results. In the selected conformations of βCN–AD, five hydrogen bonds were observed and the RMSF outlines reveal negligible movement of ligands from their poses during the MD simulation. The results of computational studies are in agreement with the experimental results as both approaches assign the same kind of binding interactions and higher binding affinity of AD.

Materials and methods

Phosphate buffer solution (10 mM, pH 7.0, containing 80 mM NaCl, with an ionic strength of 0.1) (PBS) was prepared. The stock solution of bovine βCN (> 99%; Sigma-Aldrich) was made up by dissolving it in the PBS. To avoid large protein aggregation the protein solution was filtered through a porous membrane. The protein concentration was determined from the absorbance at 280 nm by a UV–Vis spectrophotometer using an extinction coefficient of 4.6 (1%) for βCN [this is the extinction coefficient on the basis of mass concentration (the absorbance of protein solution with weight concentration of 1% equals to 4.6)]. AD was purchased from Merck Company and AA-AD (purity not less than 97%, HPLC check) was synthesized according to the literature [23] and stored only as ethanol stocks under argon atmosphere at − 52 °C. UV spectra: AA-AD λ_{max} = 282 nm (ε = 2770, ethanol).

Due to the low water solubility of ligands; their solutions were made up by dissolving them in ethanol. The exact concentration of these two solutions was measured by determining light absorption at λ_{max} = 279 nm and extinction coefficient (ε) of 3981.1 M^{-1} cm^{-1} for AD and λ_{max} = 282 nm (ε = 2770 M^{-1} cm^{-1}, ethanol) for AA-AD. All of the solutions were prepared using double-distilled water and were used freshly after preparation.

Fluorescence spectroscopy

We performed fluorescence measurements on a RF-5000 spectrofluorimeter (Shimadzu, Japan) equipped with a xenon lamp source, a 1.0-cm quartz cell and a thermostat bath that keeps temperature constant within ± 0.1 °C. In our experiments, 2 cm^3 of βCN solution (16.30 μM) was put in quartz cell and titrated with specified volumes of AD stock solution. Emission spectra were recorded from 300 to 450 nm at an excitation wavelength of 295 nm. The spectrofluorometric titration experiments were run at four different temperatures from 293 to 308 K. Both excitation and emission slit widths were set at 5 nm and control experiment was done on βCN micelle without AD. Ethanol concentration did not exceed 1% v/v during the fluorescence measurements. A similar procedure has been used for running the spectrofluorometric titration experiments for AA-AD with βCN. In these measurements, the emission spectra were recorded from 290 to 430 nm, the concentration of βCN solution and excitation wavelengths were 9.60 μM and 280 nm, respectively. The obtained data were used for binding and thermodynamic analysis.

Preparation of βCN, AA and AA-AD structures

There is no crystal structure of βCN in protein data bank; hence, homology modeling techniques and I-Threading ASSEmbly Refinement (I-TASSER) server were used to build its structure. Structural templates are first identified from PDB by multiple threading approach LOMETS; full-length atomic models are then constructed by iterative template fragment assembly simulations. Finally, function insights of the target are derived by threading the 3D models through protein function database BioLiP. The structure of βCN which was made with I-TASSER server consists of 1 helix and 5 strands and other positions were made up of random coils. Better and more stable structure can be achieved by running a molecular dynamic simulation on the proposed model of I-TASSER. For this purpose, a 50-ns molecular dynamic simulation was performed on the βCN structure using GROMACS 4.5.4 software package and the final constructed structure was used as the beginning point of molecular docking calculations.

Finally, to get the optimized and stable geometry of ligands, AD and AA-AD, the structure-optimizing calculations were carried out at the 6-31G** level by employing the Becke three-parameter Lee–Yang–Parr (B3LYP) hybrid density functional theory using the quantum chemistry software Gaussian 03 [24].

Molecular dynamics simulation

GROMACS 4.5.4 package with the GROMOS96 43a1 force field [25] and the SPC water model [26] was employed to carry out the MD simulations. First, protein was solvated in a cubic box with periodic boundary conditions, and then an appropriate number of Na^+ counterions were added instead of solvent molecules to neutralize the system. Steepest descent method [27] was employed to relax the system, energy minimization and ease from unfavorable interactions. To equilibrate the systems at 300 K, a 100-ps MD simulation in the NVT ensemble with the Berendsen thermostat coupling method was run. After stabilization of temperature an isothermal–isobaric ensemble (NPT) with the constant pressure of 1.0 bar and time duration of 100 ps was performed by employing Berendsen barostat. The Particle Mesh Ewald (PME) method [28] with 1.0-nm cutoff was used for long-range electrostatics. For van der Waals interactions, Lennard-Jones potential with 1.0-nm cutoff was employed. Finally, a 40-ns MD simulation was done to record trajectories using the leap-frog algorithm [29] to solve the equations of motion with a time step of 2 fs.

Molecular docking calculation

To find the best pose of ligands on protein, molecular docking calculation was done using Autodock 4.2 software. Hydrogens were added to the protein and during docking the macromolecule was kept rigid, while all the torsional bonds of ligands were set free to rotate. First, a blind docking was done with grid size of 126 × 126 × 126 along *X*-, *Y*-, and *Z*-axes; then the dimensions of grid map around the binding site which was found from blind docking were reduced and a grid size of 60 × 60 × 60 was constructed with a grid point spacing of 0.375 Å. Lamarckian genetic algorithm (LGA) method for 200 docking runs with 25,000,000 energy evaluations for each run and AutoDock empirical free energy function were used. The docking results were clustered with a tolerance criterion of 2.0 Å and the structure with lowest free energy of binding in the highest populated cluster was chosen as the optimal docking pose. The binding pose and important residues of protein that involved in the binding can be determined from docking results but dynamics of binding process and conformational changes during the binding cannot be understood from docking; hence, MD simulations of protein in the presence and absence of ligands were performed in which the topology parameters of protein were created from the GROMACS program and the force field parameters of ligands were taken from PRODRG web server [30].

References

1. Goodall M, Kirshner N (1958) Circulation 17:366
2. Armstrong MD, Mcmillan A, Shaw KN (1957) Biochim Biophys Acta 25:422
3. Rhoades R, Bell D (2009) Medical physiology: principles for clinical medicine. Lippincott Williams & Wilkins, Philadelphia
4. Bezuglov V, Bobrov M, Gretskaya N, Gonchar A, Zinchenko G, Melck D, Bisogno T, Di Marzo V, Kuklev D, Rossi JC, Vidal JP, Durand T (2001) Bioorg Med Chem Lett 11:447
5. Huang SM, Bisogno T, Trevisani M, Al-Hayani A, De Petrocellis L, Fezza F, Tognetto M, Petros TJ, Krey JF, Chu CJ, Miller JD, Davies SN, Geppetti P, Walker JM, Di Marzo V (2002) Proc Natl Acad Sci USA 99:8400
6. Tanasescu R, Constantinescu CS (2010) Immunobiology 215:588
7. Izzo A, Fezza F, Capasso R, Bisogno T, Pinto L, Iuvone T, Esposito G, Mascolo N, Di Marzo V, Capasso F (2001) Br J Pharmacol 134:563
8. Kunos G, Batkai S, Offertaler L, Mo F, Liu J, Karcher J, Harvey-White J (2002) Chem Phys Lipids 121:45
9. Mechoulam R (2002) Prostaglandins Leukot Essent Fat Acids 66:93
10. Shpigelman A, Israeli G, Livney YD (2010) Food Hydrocoll 24:735
11. Taheri-Kafrani A, Choiset Y, Faizullin DA, Zuev YF, Bezuglov VV, Chobert JM, Bordbar AK, Haertle´ T (2011) Biopolymers 95:871
12. Kunz C, Lo¨nnerdal B (1990) Am J Clin Nutr 51:37
13. De Kruif CG, Grinberg VY (2002) Colloids Surf A Physicochem Eng Asp 210:183

14. O'Connell JE, Grinberg VY, De Kruif CG (2003) J Colloid Interface Sci 258:33
15. Semo E, Kesselman E, Danino D, Livney Y (2007) Food Hydrocoll 21:936
16. Mehranfar F, Bordbar A-K, Parastar H (2013) J Photochem Photobiol B Biol 127:100
17. Lakowicz JR (2006) Principles of fluorescence spectroscopy. Springer, New Jersey
18. Min J, Meng-Xia X, Dong Z, Yuan L, Xiao-Yu L, Xing C (2004) J Mol Struct 692:71
19. Mehranfar F, Bordbar A-K, Fani N, Keyhanfar M (2013) Spectrochim Acta Part A Mol Biomol Spectrosc 115:629
20. Mehranfar F, Bordbar A-K, Amiri R (2015) Biomacromol J 1:69
21. Eftink MR, Ghiron CA (1981) Anal Biochem 114:199
22. Pertwee RG (2006) Br J Pharmacol 147:163
23. Bezuglov VV, Manevich Y, Archakov AV, Bobrov MY, Kuklev DV, Petrukhina GN, Makarov VA, Buznikov GA (1997) Bioorg Khim 23:211
24. Frisch MJG, Trucks W, Schlegel HB, Scuseria GE, Robb MA, Cheeseman JR, Montgomery JA, Vreven T Jr, Kudin KN, Burant JC, Millam JM, Iyengar SS, Tomasi J, Barone V, Mennucci B, Cossi M, Scalmani G, Rega N, Petersson GA, Nakatsuji H, Hada M, Ehara M, Toyota K, Fukuda R, Hasegawa J, Ishida M, Nakajima T, Honda Y, Kitao O, Nakai H, Klene M, Knox X, Li JE, Hratchian HP, Cross JB, Adamo C, Jaramillo R, Gomperts RE, Stratmann O, Yazyev AJ, Austin R, Cammi C, Pomelli J, Ochterski JW, Ayala PY, Morokuma K, Voth GA, Salvador P, Dannenberg JJ, Zakrzewski VG, Dapprich S, Daniels AD, Strain MC, Farkas O, Malick DK, Rabuck AD, Raghavachari K, Foresman JB, Ortiz JV, Cui Q, Baboul AG, Clifford S, Cioslowski J, Stefanov BB, Liu G, Liashenko A, Piskorz P, Komaromi I, Martin RL, Fox DJ, Keith T, Al-Laham MA, Peng CY, Nanayakkara A, Challacombe Gill PMW, Johnson B, Chen W, Wong MW, Gonzalez C, Pople JA (2004) GAUSSIAN 03 (Revision B.02). Gaussian, Inc, Wallingford
25. Van Der Spoel D, Lindahl E, Hess B, Groenhof G, Mark AE, Berendsen HJ (2005) J Comput Chem 26:1701
26. Rivail L, Chipot C, Maigret B, Bestel I, Sicsic S, Tarek M (2007) J Mol Struct THEOCHEM 817:19
27. Hess B, Bekker H, Berendsen HJC, Fraaije JGEM (1997) J Comput Chem 18:1463
28. Essmann U, Perera L, Berkowitz ML, Darden O, Lee H, Pedersen LG (1995) J Chem Phys 103:8577
29. Morris GM, Goodsell DS, Halliday RS, Huey R, Hart WE, Belew RK, Olson AJ (1998) J Comput Chem 19:1639
30. van Aalten DMF, Bywater R, Findlay JBC, Hendlich M, Hooft

RWW, Vriend G (1996) J Comput Aided Mol Des 10:255